AGU ADVANCING EARTH AND SPACE SCIENCES

JGR Space Physics

RESEARCH ARTICLE
10.1029/2026JA035427

Can Solar Cyclic Variability Mimic Extreme Solar Particle (Miyake) Events in Radiocarbon?

Ilya Usoskin[1,2], **Fusa Miyake**[2], **and Kseniia Golubenko**[1]

[1]Space Physics and Astronomy Research Unit and Sodankylä Geophysical Observatory, University of Oulu, Oulu, Finland,
[2]Institute for Space-Earth Environmental Research, Nagoya University, Nagoya, Japan

Key Points:

- Detectability of Miyake events in ^{14}C was tested with the SOCOL:14C-Ex model
- Solar cycles and trends in $\Delta^{14}C$ can distort and mimic weak–moderate Miyake events
- Measurements of solar cycles and trends are needed to study weak Miyake events

Supporting Information:

Supporting Information may be found in the online version of this article.

Correspondence to:

I. Usoskin,
ilya.usoskin@oulu.fi

Citation:

Usoskin, I., Miyake, F., & Golubenko, K. (2026). Can solar cyclic variability mimic extreme solar particle (Miyake) events in radiocarbon? *Journal of Geophysical Research: Space Physics*, *131*, e2026JA035427. https://doi.org/10.1029/2026JA035427

Received 28 MAR 2026
Accepted 6 AUG 2026

Abstract

Rapid, strong enhancements in $\Delta^{14}C$ in the Earth's atmosphere, known as Miyake events, rarely occurred over the past millennia, pointing to major radiation storms affecting Earth. They are produced by extreme solar particle events (ESPEs) and are separated by an order-of-magnitude gap in the strength from directly observed solar particle storms. This leaves their physical interpretation unconstrained. To bridge this gap, weak–moderate Miyake events ought to be detected, but this possibility was previously limited by the accuracy of individual ^{14}C measurements. Here, we performed a sensitivity study of the detectability of a Miyake event in radiocarbon data over the background of natural $\Delta^{14}C$ variability. The study was done for realistic conditions, including a reference ESPE, using the SOCOL:14C-Ex (SOlar CLimate Ozone Links model, radiocarbon version for extreme solar proton events) model of carbon transport in the Earth's atmosphere. We found that background variability, such as long-term trends and the solar cycle, can significantly distort and even mimic weak-to-moderate Miyake events in radiocarbon data. We conclude that reducing measurement errors alone is not sufficient to identify such weaker events. In addition, the galactic cosmic ray (GCR)-related background should be reconstructed over ≈50 years around event candidates using high-precision annual measurements of $\Delta^{14}C$.

1. Introduction

The Sun is a moderately active star with variable magnetic activity, including both a regular cyclic component and sporadic energetic eruptive phenomena (Hathaway, 2015). Solar activity was extensively studied by direct scientific measurements for the last decades, by photographic images for a century, and by visual observations for about 400 years. Of particular importance for terrestrial effects (Calisto et al., 2013; Golubenko et al., 2020; Sukhodolov et al., 2017) are energetic events leading to the acceleration of solar energetic particles (SEPs) whose flux can significantly exceed the omnipresent background of galactic cosmic rays (GCRs) for hours–days. The physics of SEP is generally understood, but the details are still missing, in particular in relation to strong events (Desai & Giacalone, 2016). However, it was discovered (Miyake et al., 2012) that the Sun can rarely produce extremely strong SEP events, commonly referred to as extreme solar particle events (ESPEs) (Miyake et al., 2020; Usoskin, 2023; Usoskin et al., 2013). These events are identified in natural archives via proxy records as sharp increases in cosmogenic isotope production, such as ^{14}C, ^{10}Be, and ^{36}Cl. The flux of energetic particles during ESPEs is so strong that a significant amount of cosmogenic isotopes is produced in the atmosphere and stored in natural archives. Such isotope anomalies are commonly termed Miyake events (Bard et al., 2023; Heaton et al., 2024; Miyake et al., 2020; Panyushkina et al., 2024). A typical Miyake event in radiocarbon is shown in Figure 1 and is characterized by a short rise of $\Delta^{14}C$, within 1–2 years, followed by a gradual decay due to the carbon cycle. To be reliably detectable in cosmogenic isotope data, ESPEs need to be several orders of magnitude stronger than directly recorded 'normal' SEP events. Known ESPE can increase the annual production of cosmogenic isotopes in the atmosphere by a factor of 2–10 over the GCR background and be observed in the isotope records with sufficiently high resolution. They seldom occur—nine ESPEs and candidates are presently known over the last 14.5 millennia, corresponding to roughly one event per 1,500–2,000 years (Cliver et al., 2022; Usoskin et al., 2023). The strongest known Miyake events took place in 774 CE (Miyake et al., 2012) and 12350 BCE (Bard et al., 2023). ESPEs have not been directly observed during the last decades. Because of that, there is an order-of-magnitude gap between the directly observed SEP events and the proxy-based Miyake events (Usoskin & Kovaltsov, 2021).

While the solar origin of the Miyake events is commonly accepted (Mekhaldi et al., 2015; Paleari et al., 2022; Usoskin et al., 2013), the exact physical mechanism of their formation remains unconstrained (Cliver et al., 2022).

10.1029/2026JA035427

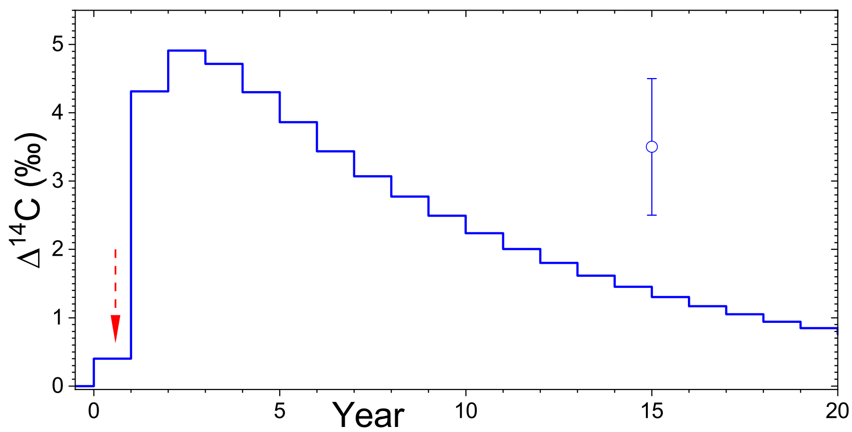

Figure 1. Modeled profile of the annual Δ^{14}C response to the reference ESPE (see Section 2.2). The red arrow indicates the ESPE date (DoY0 213, 1 August 1865 CE). Synthetic error bars ($\sigma_C = 1.0$‰) are shown in blue.

It was discussed that the energetics of such events might be beyond the Sun's ability to release energy in solar flares (Aulanier et al., 2013). A very important question is whether ESPEs are *Black Swans*, viz., the extreme tail of the distribution of standard SEP events strength, or *Dragon Kings*, viz., events of the presently unknown type with the occurrence probability and strength distribution unrelated to those of the directly observed events (Cliver et al., 2022; Usoskin et al., 2023). In the Black Swan case, dozens of moderate and weak Miyake events could be discovered over the Holocene, while in the Dragon King case, their number should be small. To answer this question, it is crucial to fill the observational gap, which can be done either by waiting for an ESPE to occur during the modern era or by studying weak-to-moderate Miyake events in the past. While the former can take centuries, the latter can be done nowadays, but is limited by the detection threshold of the cosmogenic-isotope method, mostly due to the measurement uncertainties of the isotopic concentrations. The earlier studies (Mekhaldi et al., 2021; Usoskin et al., 2020), which considered an ideal case of a pure Miyake event, concluded that higher-precision measurements and multi-proxy data can reduce the noise and thus the threshold. In reality, however, Miyake events occur on a variable GCR-related background, which includes long-term trends and solar-cycle variations. Since these variations are natural, they cannot be removed by more precise measurements or multi-proxy data sets and require full consideration.

Here, we consider the possibility that the GCR-related background in the radiocarbon data can distort or even mimic the occurrence of the Miyake events, potentially leading to the false identification of ESPEs in realistic data.

2. Modeling of Radiocarbon Production

For direct modeling of the Δ^{14}C concentrations, we used the following approach based on several steps.

2.1. Background Production by GCR

Since the level of radiocarbon Δ^{14}C in tree rings and near-ground air at the time of the tree growth depends not only on the momentary production rate of ^{14}C but also on the carbon production and exchange in large slow reservoirs like the ocean for the preceding millennia, we considered a realistic history of radiocarbon production for 10 millennia into the past (Roth & Joos, 2013; Wu et al., 2018). This pseudo-annual production interpolated from decadal data does not resolve individual solar cycles. Using this production and the 11-box carbon cycle model (Büntgen et al., 2018), we have modeled the equilibrium partition of ^{14}C over the 11 boxes (reservoirs) for the year 1000 CE. For the past millennium, we used annually resolved production variability, reconstructed recently (Brehm et al., 2021; Usoskin et al., 2021). This includes individual solar cycles and forms the basic production profile as shown in Figure 2.

For individual scenarios (see Section 3), the radiocarbon production by GCR was modeled, on the time scale of a few decades, using the CRAC:14C (Cosmic Ray Atmospheric Cascade model, version for radiocarbon—Poluianov et al., 2016) based on the force-field modulation potential ϕ (Usoskin et al., 2005, 2017).

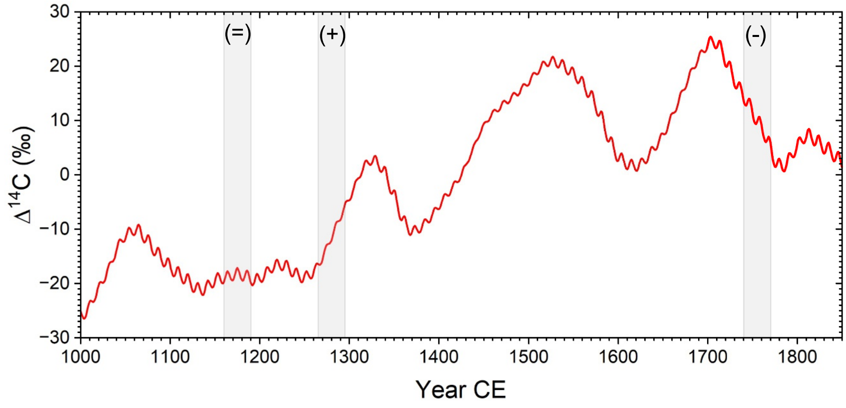

Figure 2. Basic Δ^{14}C profile for the past millennium (see Section 2.1). Vertical gray bars denote the periods considered for the trends, as summarized in Table 1.

Realistic variable geomagnetic dipole moment strength (Usoskin et al., 2016) was used for the ^{14}C production computations. While there are alternative paleomagnetic models (Panovska et al., 2023; Pavón-Carrasco et al., 2014), we did not consider them in this sensitivity study, since the geomagnetic changes are slow and can be neglected at the timescale considered. With this scenario-related production, we replaced the actual production profile for the period of interest. The values of Δ^{14}C were calculated using the carbon-cycle box model (Büntgen et al., 2018) for the past millennium, with the pre-computed equilibrium carbon reservoir partition as the boundary conditions for the year 1000 CE, as described above.

For the modeled Δ^{14}C values, a synthetic error bar of σ_C was added to simulate the measurement uncertainties. This corresponds to an optimistic statistical error of a single sample measurement (e.g., Miyahara et al., 2022). For the main scenario, an optimistic $\sigma_C = 1‰$ was applied, but for sensitivity studies, it varied between 0.2 and 1.5‰.

For the numerical experiments, we used the following modeled scenarios, involving possible combinations of three production scenarios, S0–S2 (see below), and three scenarios for the Δ^{14}C background trend, denoted as (−)—negative trend, (=)—no trend, and (+)—positive trend. For example, S1(=) denotes production scenario 1 applied to the no-trend conditions.

The Δ^{14}C trends, represented for the past millennium, are summarized in Table 1 and shown in Figure 2. The largest negative trend of $-0.25‰\ yr^{-1}$ was observed around 1750 CE and corresponded to the recovery after the Maunder minimum. The period with a stable Δ^{14}C concentration was observed around 1180 CE between the Oort and Wolf grand minima. A large positive trend of about $0.5‰\ yr^{-1}$ was observed around 1290 CE at the beginning of the Wolf grand minimum. This trend is close to the maximum possible GCR-related trend of $\approx 0.7‰$ yr^{-1}, theoretically expected for the lack of solar modulation ($\phi = 0$) and weak geomagnetic field $M = 6 \cdot 10^{22}$ at m^2. The strongest negative trend for a hypothetical instant switch-off of cosmic rays (no production of ^{14}C) would be -(1–1.2) ‰ yr^{-1}.

The following three scenarios for the GCR-related production of ^{14}C were considered, as shown in Figure 3:

Table 1
Trends and Production Scenarios in Δ^{14}C Considered Here

Trends			GCR scenarios			ESPE scenarios		
Trend	Value	Period CE	S0	S1	S2	x0.5	x1.0	x1.5
Negative (−)	−0.25	1740–1770	S0(−)	S1(−)	S2(−)	–	–	–
No trend (=)	0	1160–1190	S0(=)	S1(=)	S2(=)	Ex0.5	Ex1.0	Ex1.5
Positive (+)	0.5	1265–1295	S0(+)	S1(+)	S2(+)	–	–	–

Note. The blocks represent the trends (name and notation, the value of the trend in ‰ yr^{-1}, and the representative period—see Figure 2); GCR scenarios; and reference ESPE scaled with factors x0.5, x1 and x1.5.

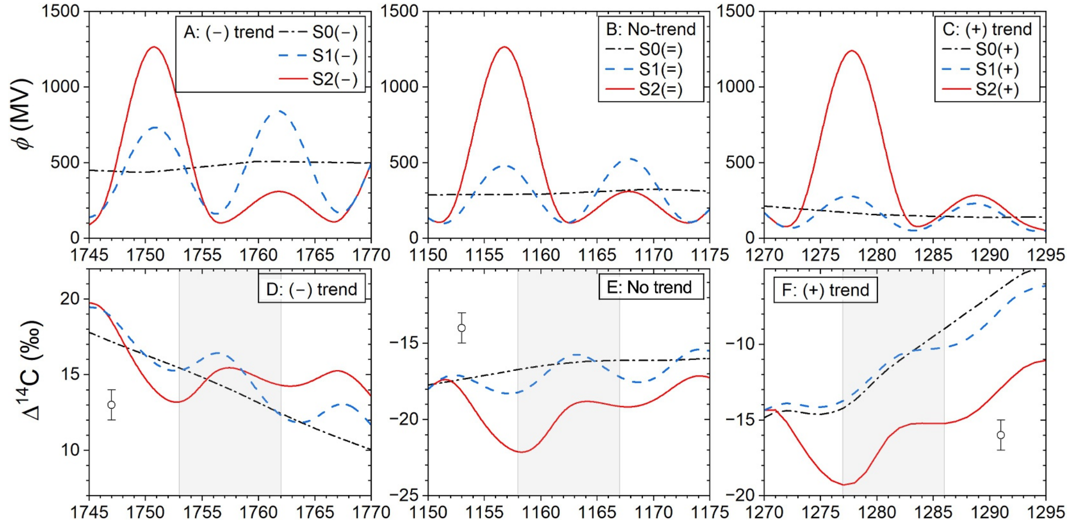

Figure 3. Upper row (panels a–c): Profiles of the modulation parameter ϕ used for different scenarios S0–S2 as depicted by different curves, and trends (Table 1) as presented at different columns. Lower row (panels d–f): Modeled $\Delta^{14}C$ profiles for the GCR-production scenarios and trends, shown in the upper panels. Gray bars depict the period subjected to the ESPE reconstruction analysis. Error bars in the lower panels indicate the synthetic uncertainties applied to the modeled series.

1. S0—No solar cycles—the modulation parameter ϕ is set as linearly interpolated between the decadal averaged value for the corresponding time period.
2. S1—Realistic solar cycles—the modulation parameter ϕ was applied as reconstructed from the real data (Usoskin et al., 2021).
3. S2—A pair of strong–weak solar cycles—an artificially strong solar cycle (ϕ_{max} = 1,300 MV) followed by a very weak cycle (ϕ_{max} = 300 MV).

2.2. Production by ESPE

For the ESPE-related production, we assumed a reference ESPE event defined as a recent (20 January 2005) impulsive hard-spectrum GLE#69 scaled up by a factor of 100 (Golubenko et al., 2025, 2026). GLE#69 was selected as the baseline because it is the most intense and best-documented solar proton event of the satellite era, and its unusually hard energy spectrum makes it a more suitable proxy for Miyake-like events. The omnidirectional integral fluence of SEPs with energy above 200 MeV for this reference event was $F_{200} = 2.78 \cdot 10^9$ cm^{-2} (Koldobskiy et al., 2021). The ESPE was assumed to occur on DoY (Day of Year) 213, viz., 1 August 1865 CE. The timing was selected to represent pre-industrial conditions before major anthropogenic perturbations of atmospheric ^{14}C, such as fossil-fuel dilution and bomb-produced radiocarbon. The year when the event took place is denoted as year 0 henceforth, and the event's date is denoted as DoY0 which is the day number relative to January 1st of year 0. The geomagnetic field was considered as $M = 9.5 \cdot 10^{22}$ A m^2, corresponding to the middle of the last millennium (Usoskin et al., 2016).

The values of $\Delta^{14}C$ were calculated for the near-ground air using the dynamical atmospheric model SOCOL:14C-Ex (SOlar CLimate Ozone Links model, radiocarbon version for extreme solar proton events—Golubenko et al., 2025; Golubenko et al., 2026) for the standard Holocene conditions with the atmospheric CO_2 concentration of 287 ppmv. The reference ESPE corresponds to the global production of about $3.7 \cdot 10^{26}$ atoms of ^{14}C in the atmosphere or 2.3 atoms per cm^2 per second over 1 year (Golubenko et al., 2025), which would more than double the annual standard pre-industrial production rate of 1.6–1.8 atoms per cm^2 per second due to GCRs (Kovaltsov et al., 2012). We assumed that the measured $\Delta^{14}C$ values directly represent the in-air concentration of ^{14}C averaged over the tree-growth season. A possible effect of tree physiology, including species type and carbon storage effects, on the measured signal (Hessl et al., 2026; Uusitalo, 2026) is supposed to be small and is neglected here.

The modeled $\Delta^{14}C$ profile for the reference ESPE is shown in Figure 1 as exemplified for a Central Europe location (44.31°N, 5.52°E), but it is similarly shaped for any other location in the Northern hemisphere

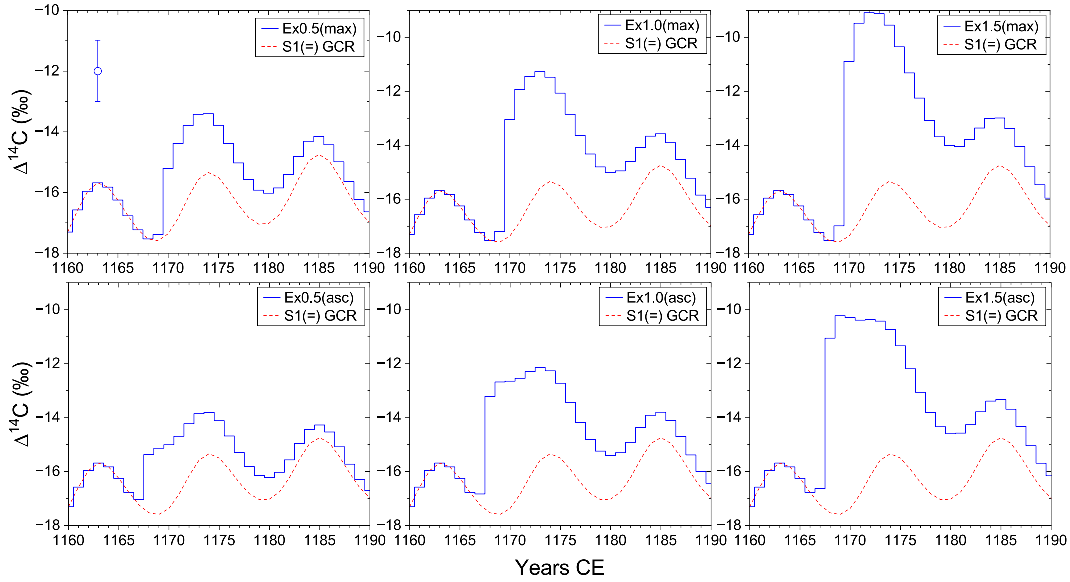

Figure 4. Modeled Δ^{14}C time profiles for ESPE + GCR scenarios for an ESPE occurring at the solar maximum (upper row, (max)-scenarios) and mid-ascending phase (lower row, (asc)-scenarios). The GCR background (dashed red lines) corresponds to the S1(=) scenario. The ESPE (blue lines) was considered as x0.5, x1, and x1.5 of the reference ESPE (Figure 1) as shown in the left, middle and right columns. The error bar on the top-left panel represents the synthetic uncertainties of the modeled data sets.

(Golubenko et al., 2025). The Δ^{14}C response to a production spike rises for about 2 years due to the stratospheric transport and stratosphere-troposphere exchange, reaching a peak of 5‰ at year 2, and then nearly exponentially decreases due to the sink of the produced radiocarbon to the surface ocean and biota. This reference event roughly corresponds to the detection limit of an ESPE by the cosmogenic-isotope method (Usoskin et al., 2020).

The ESPE-related signal was considered additive with respect to the GCR-based Δ^{14}C profiles for different scenarios.

2.3. Combination of ESPE and GCR Production

We also checked a set of scenarios with a combination of the ESPE and GCR modulation cycles. As the GCR scenario, we first considered S1(=), viz., realistic cycles with no trend as exemplified for the period around 1170 CE. For the ESPE, we considered an additive scenario, where the reference ESPE signal, shown in Figure 1, was scaled with a factor of x0.5, x1.0, and x1.5, and added on top of the GCR scenario. The corresponding scenarios are referred to as Ex0.5, Ex1.0, and Ex1.5, respectively. Two possible dates of ESPE were taken as corresponding to the solar-cycle maximum and mid-ascending phase, as denoted with the suffix "(max)" or "(as)," respectively. For example, the scenario Ex0.5(as) corresponds to the reference ESPE, scaled by a factor of 0.5 and occurring during the ascending phase, on top of the S1(=) GCR scenario. These two cases bound the possible range of solar-cycle effects on the event's detectability, from hiding to enhancing or even mimicking the event in the data. The corresponding time profiles of Δ^{14}C are shown in Figure 4.

2.4. Reconstruction of the ESPE Parameters

From the synthetic Δ^{14}C data sets, a reconstruction of the parameters of the parent ESPE was performed by applying the MCMC (Markov Chain Monte Carlo) method, briefly described below (Golubenko et al., 2026).

1. First, we produced a randomized synthetic data set $X_{i,j} = D_{i,j} + R_{\rm n} \cdot \sigma_{\rm C}$, where $D_{i,j}$ and $\sigma_{\rm C}$ are the modeled Δ^{14}C values for a given scenario and the standard error, respectively, as described above. Indices i and j correspond to the number of the data set and the year of the modeled time interval, respectively, and $R_{\rm n}$ is a normally distributed random number with zero mean and unit dispersion.

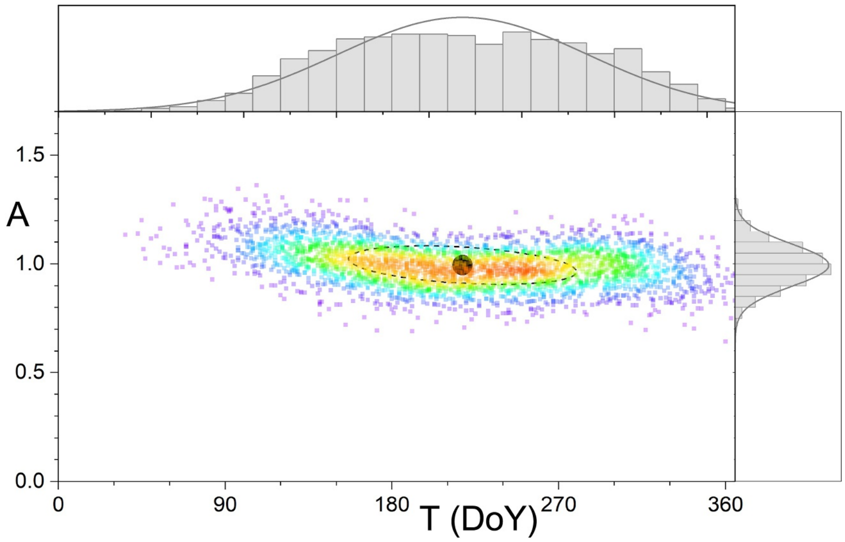

Figure 5. Example of the reconstruction of the reference ESPE from synthetic noisy data by the MCMC method (Section 2.4). The central panel shows the color-coded distribution density of 3000 MCMC simulations in the A-versus-T parameter space. Distributions of T and A values are shown on the top and right panels, respectively, along with the best-fit Gaussians. The black circle and black-dashed oval denote the gravity center ($A = 0.995$ and $T = 218$ DoY0) and the 68% confidence area, respectively, of the reconstructed parameters.

2. Second, the possible event's date T was scanned, with a daily cadence, for several years around the supposed event year. For each scanned year j, the corresponding precomputed ESPE model curve $\mathcal{D}_j$ was considered (Golubenko et al., 2026), similar to that shown in Figure 1 for DoY0 = 213. The synthetic data set $\tilde{X}_i$ was fit linearly by the fitting curve $\tilde{\mathcal{D}}^*(T)$ and finding the best-fit values of the offset C_0 and scaling factor A, as $\tilde{X}_i = A \cdot \tilde{\mathcal{D}}^*(T) + C_0$. The date T_i and scaling factor A_i, corresponding to the minimum RMSE (root mean squared error) between the synthetic data sets and the fit, were recorded for each case.
3. Steps 1 and 2 were repeated $N = 3000$ times, by using a new set of random numbers R_n at each time, producing a pool of best-fit parameter values A_i and T_i. From these distributions, the mean values and the standard deviations were computed as estimates for the reconstructed ESPE strength and timing.

An example of the MCMC-based reconstruction of the ESPE parameters is shown in Figure 5 for the noised reference event Ex1.0 occurred on DoY0 213 shown in Figure 1. Despite large error bars, the method accurately reconstructs the parameters of the ESPE, as $A = 0.995 \pm 0.09$ and $T = 218 \pm 65$, confirming the validity of the approach.

We also checked whether the reduced error bars would improve the reconstruction of the ESPE parameters. The results of the reconstruction are summarized in Table 2 for different event strengths and different synthetic error bars. As seen, the strength of the modeled event, A, is reconstructed correctly, even for small ESPEx0.2 events and large error bars of 1–1.5‰. However, the event's occurrence date can be reconstructed only for stronger events, $A > 0.5$, and smaller error bars $\sigma < 0.5$‰. Thus, we can conclude that the MCMC method works well, and weak ESPEs of x0.5 or even x0.2 can be potentially identified and reconstructed with the help of reducing the measurement errors. However, we note that this exercise was done for the undisturbed event, while the variable background of GCR-related radiocarbon may distort the ESPE signal, as discussed below.

3. Results

Here, we analyse the results of the formal reconstruction of the ESPE parameters by the MCMC-based reference curve fitting (Section 2.4) for different scenarios and trends.

3.1. GCR Modulation

First, we analysed the results of the formal reference-curve fitting to the purely GCR-modulated signal as described in Section 2.1 and shown in Figure 3. We emphasize that these scenarios do not involve a Miyake event,

Table 2
Reconstruction of the Modeled Ideal ESPE, viz. the Reference Event (A = 1.0 Occurred at Day T = 213 DoY0–1 August 1865 CE), Scaled as x1.0, x0.5, and x0.2, From the Synthetic Data With the Measurement Errors σ

ESPE	Ex1.0		Ex0.5		Ex0.2	
σ	A	T (DoY0)	A	T (DoY0)	A	T (DoY0)
1.5‰	1.02 ± 0.15	N/A	0.52 ± 0.15	N/A	0.20 ± 0.15	N/A
1.0‰	1.00 ± 0.09	218 ± 65	0.52 ± 0.10	N/A	0.21 ± 0.10	N/A
0.5‰	1.00 ± 0.05	215 ± 46	0.50 ± 0.05	208 ± 71	0.20 ± 0.05	N/A
0.2‰	0.99 ± 0.02	212 ± 26	0.49 ± 0.02	212 ± 43	0.20 ± 0.02	212 ± 74

Note. The values in columns depict the ESPE parameters reconstructed by the MCMC method (Section 2.4). The values for Ex1.0 and $\sigma = 1$‰—correspond to Figure 5. N/A denotes that the event's date cannot be reconstructed.

by construction. The results are summarized in Table 3, and the parameter distributions, similar to Figure 5, are shown in Figure S1. As seen, the fit produces some formal results, in particular, for the event magnitude A. However, the event's date T cannot be defined even formally, as the values of T are spread over the entire year.

For scenario S0, viz., no solar cycles, the formal values of A are defined by the trend, being significantly negative (−0.25 ± 0.14—see Table 3), consistent with zero (0.02 ± 0.14), and significantly positive (0.29 ± 0.13), for scenarios S0(−), S0(=), and S0(+), respectively. The value of T (the event's date) remains unsettled. Thus, the trend in $\Delta^{14}C$ can affect the reconstructed strength of the Miyake event within ±0.3 of the reference events.

For scenario S1 (realistic solar cycles), the solar-cycle variability defines the reconstructed event's magnitude A, which appears about 0.2, 0.25, and 0.4 (see Table 3) for the negative, no, and positive trends, respectively. As seen, the trend can reduce (negative trend) or enhance (positive trend) the cycle variability. Still, the event's date cannot be defined, with the values of T covering the entire year.

For the S2 scenario (a strong solar cycle followed by a weak one), significant formal A values were obtained, ranging from about 0.4 (negative trend) to 0.6 (positive trend). The reconstruction is dominated by the solar-cycle variability, with the trend slightly affecting its magnitude. The event's date cannot be reconstructed.

In these analyses, the event's year was automatically defined to match the profiles best. Since there was no event in the data, by construction, all these reconstructions should be considered as false positive, viz., the GCR variability mimicking the event. These simulations were performed for moderate measurement error bars of σ =1‰, but we also checked that reducing the error bars would not improve the situation. For example, the reconstruction for the S1(+) scenario yields $A = 0.38 \pm 0.06$ for the $\sigma = 0.5$‰ which is nearly the same as the results in Table 3 for the same scenario, but for $\sigma = 1$‰.

3.2. ESPE Over the GCR Background

Another set of scenarios was related to a simulated Miyake event produced by the reference ESPE, which was added on top of the variable GCR background as specified in Section 2.3. The modeled ESPE was considered to occur at DoY0 213, as Ex0.5, Ex1.0, and Ex1.5 scenarios, and we checked if the method reconstructs it correctly.

Table 3
The Magnitude A of the Formally Reconstructed Miyake Events (see Figure S1) for Scenarios S0(−) Through S2(+) With GCR Variability Only, viz., no ESPE—see Table 1 for Definitions

	Trend		
Scenario	Negative	No-trend	Positive
S0	−0.25 ± 0.09	0.05 ± 0.09	0.29 ± 0.09
S1	0.18 ± 0.09	0.39 ± 0.10	0.38 ± 0.10
S2	0.44 ± 0.09	0.49 ± 0.10	0.58 ± 0.10

Note. Date of the event T cannot be defined in these cases.

Table 4
Parameters of the Simulated ESPE (Magnitude as Specified in Scenarios in Table 1, and Date of 213 DoY0–1 August 1865 CE) and Its Reconstructions: The Reconstructed Magnitude A, and the Event's Date

	Maximum phase		Ascending phase	
Scenario	A	T (DoY0)	A	T (DoY0)
Ex0.5	0.74 ± 0.11	415 ± 60	0.44 ± 0.11	N/A
Ex1.0	1.19 ± 0.11	361 ± 41	0.90 ± 0.12	341 ± 57
Ex1.5	1.66 ± 0.12	334 ± 31	1.38 ± 0.11	307 ± 38

Note. Details of the reconstruction are shown in Figure S2.

First, we placed the modeled event at the maximum phase of the solar cycle as shown in Figure 4 upper row of panels. The results of the formal fitting are shown in Table 4 and Figure S2. The magnitude of the event is reconstructed robustly, but it appears overestimated by about 0.2, because of the solar cycle adding its own magnitude to the event's strength (see Figure 4). This addition is nearly constant for the different modeled events' strengths. The reconstructed event timings are shifted toward later dates, from 2 to 3 months for the Ex1.5 event to about 6 months for the Ex0.5 event.

Next, the modeled event was placed at the middle of the ascending phase of the solar cycle (Figure 4, bottom row). In this case, the magnitude of the reconstructed event appears to be underestimated by about 0.1, because of the solar cycle now reducing the event's peak. The reconstructed event's date is delayed by 3 months for the x1.5 event, 4 months for the x1 event, and becomes unrecognizable for the x0.5 event.

We also artificially reduced the error bars of the synthetic $\Delta^{14}C$ data set from 1 to 0.5‰. It didn't modify the reconstructed parameters shown in Table 4, but only slightly reduced the formal uncertainties. For example, the reconstructed parameters of the Ex1.0(max) scenario were found as $A = 1.19 \pm 0.06$ and $T = 361 \pm 21$ for $\sigma = 0.5$‰ (cf. $A = 1.19 \pm 0.11$ and $T = 361 \pm 41$ for $\sigma = 1$‰—see Table 4). Despite the reduced formal uncertainties, the reconstructed parameters are far from those for the true reference event. This implies that the distortion of the Miyake event's shape by the solar cycle cannot be resolved solely by the improved accuracy of data sets, but requires identification of and correction for the GCR-background variability.

3.3. Example of the Correction for the ESPE of 1279 CE

We illustrate this methodology on an example of the ESPE-event candidate of 1279 CE in the annual radiocarbon data from Brehm et al. (2021) as shown in Figure 6a (dots with error bars). That was a period of a systematically rising trend in $\Delta^{14}C$ because of the beginning of the Wolf grand solar minimum (Usoskin et al., 2007). The Miyake-event candidate occurred around 1280 CE, against the background of a cyclically variable GCR effect. To account for that, we have fitted a sinusoidal wave superimposed on a linear trend to the annual $\Delta^{14}C$ data for the period 1260–1278 and 1290–1310 CE, viz. not affected by the event. The fit was interpolated for the period 1279–1289 CE as shown by the red line in Figure 6a. The best-fit parameters were found as follows: the sine wave's period, phase and amplitude are 9.7 years, 1.134 rad, and 1.3‰, respectively, and the slope 0.33‰ yr^{-1}. We note that this is an approximate fitting since the solar cycles are not purely periodic and sinusoidal, but it indicates a phase of the cycles. By removing the fitted trend from the actual data, we obtained a detrended data set shown in Figure 6b. The error bars, corresponding to the measurement uncertainties and the trend definition, were summed quadratically.

Next, we estimated the parameters of the ESPE, following the MCMC approach (Section 2.4) for both original and detrended data sets. The formal ESPE fitted to the original data set (Figure 6a) was found as $A = 1.22 \pm 0.20$ (peak 6.1‰) with the event date being $T = 204 \pm 86$ DoY 1279 CE. For the detrended data set (panel b), the estimated parameters of the event were $A = 0.92 \pm 0.21$ (peak 4.5‰), and $T = 180 \pm 80$ DoY. The event in the raw data appeared significantly, by about 30%, stronger than that in the detrended data. We emphasize that this exercise doesn't pretend to be a full analysis, because of the single data set used, and a simplified modeling, but it illustrates that the variable background may distort the Miyake-event candidates.

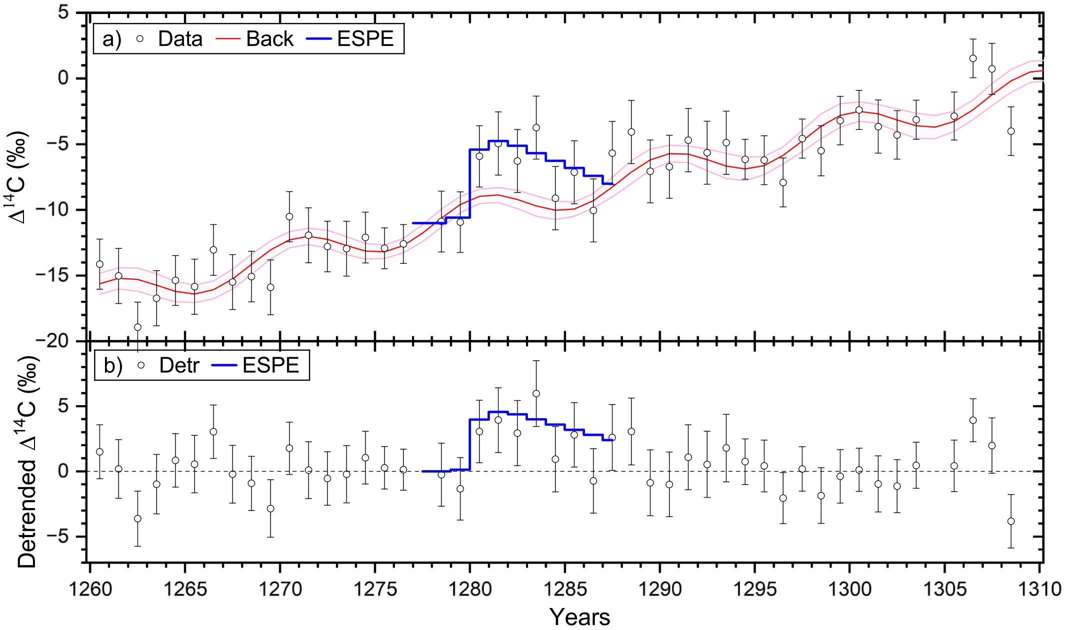

Figure 6. Radiocarbon variability around 1279 CE. Panel (a) annual Δ^{14}C data (Brehm et al., 2021), best-fit background of a sinusoid (period 9.7 years, amplitude 1.3‰—red curve), and the best-fitted ESPE curve (A = 1.22). Panel (b) detrended annual Δ^{14}C data (dots), viz. data minus trend—see panel (a), and the best-fit ESPE curve (A = 0.92).

4. Summary and Conclusions

With the modeling and subsequent reconstruction of the synthetic ESPE-caused Miyake events, we analysed the robustness of the event reconstruction against the background variations in Δ^{14}C due to GCR. The latter includes 11-year solar cycles and long-term trends related to grand solar minima.

First, we checked whether the GCR-related variability can mimic a Miyake event. An analysis of several scenarios (see Table 3), where the event was not present in the input data, implies that both long-term trends and solar-cycle variability can mimic Miyake events in the Δ^{14}C data. The maximum effect gives a combination of a strong positive trend in Δ^{14}C of up to 0.5‰ yr^{-1}, which is typical for the beginning of a solar grand minima, on one hand, and a strong solar cycle followed by a weak one (scenario S2(+)—see Table 1), on the other hand. This combination can lead to a spurious identification of an ESPE with the magnitude of x0.6 of the reference one. The event's date cannot be established in this case. Accordingly, we conclude that ESPEs with the magnitude below x0.5–x0.7 of the reference event cannot be robustly identified, if the background solar-cycle variability is unknown a priori. This might be the case for a Miyake-event candidate of 1279 CE (Miyake et al., 2026).

Next, we studied how solar-cycle variability can affect the identification of an ideal ESPE in the simulated data. The results, summarized in Table 4, imply that weak events, x0.5 of the reference ESPE, can be strongly distorted by the background variability, so that the magnitude A can be offset by about x0.2 with the event's date being completely lost. Stronger events, x1.0 or x1.5 of the reference ESPE, can be robustly identified in both magnitude and date, but with a biased magnitude of ±x0.2 depending on the solar-cycle phase, and the event date potentially offset by several months.

Based on the presented analysis, we conclude that a quantitative study of weak–moderate Miyake events requires taking into account the background Δ^{14}C variability, including the long-term trend and the solar cycle. While the trends can be established from the coarser-resolution data, for example, the IntCal data set (Reimer et al., 2020), the account of solar cycles requires precise annual measurements of Δ^{14}C for a few decades before the event, and about 30 years after that, viz., about 50 annual datapoints around the event. This is important for moderate events, with the magnitude of x1–x2 of the reference ESPE, and becomes crucial for weaker events. Events with the magnitude below x0.7 of the reference ESPE cannot be robustly identified without an analysis of the background variability. We note that reducing the measurement errors alone is not sufficient to identify such weaker ESPEs, but the GCR-related background should be reconstructed around the event candidates. We propose that a 50-year period around the Miyake event candidates ought to be covered by high-precision annual measurements of $\Delta^{14}C$ for a reliable identification of the events and reconstruction of their parent ESPE parameters.

The present level of the radiocarbon measurement accuracy makes reliable detection of weak or moderate ESPEs difficult and does not allow for distinguishing between Black Swan and Dragon King scenarios.

Conflict of Interest

The authors declare no conflicts of interest relevant to this study.

Availability Statement

No restriction on data availability applies to the data we used. All statistical analyses and data processing were performed using the MATLAB software environment and its standard statistical toolboxes. The study also employed the CCM SOCOL:14C-Ex model (Golubenko et al., 2025).

Acknowledgments
This work was partly supported by the European Research Council Synergy Grant (project 101166910). F.M. acknowledges support from JSPS (Grants. JP20H05643 and JP25H00635) and MEXT (Grant JPMXP1324134720). I.U. acknowledges partial support from ERC Synergy Grant (project 101166910 GERACLE). The ISSI Teams 510 (SEESUP, led by F. Miyake and I. Usoskin) is acknowledged for stimulating discussions. Open access publishing facilitated by Oulun yliopisto, as part of the Wiley - FinELib agreement.

References

Aulanier, G., Démoulin, P., Schrijver, C. J., Janvier, M., Pariat, E., & Schmieder, B. (2013). The standard flare model in three dimensions. II. Upper limit on solar flare energy. *Astronomy and Astrophysics*, *549*, A66. https://doi.org/10.1051/0004-6361/201220406

Bard, E., Miramont, C., Capano, M., Guibal, F., Marschal, C., Rostek, F., et al. (2023). A radiocarbon spike at 14300 cal yr BP in subfossil trees provides the impulse response function of the global carbon cycle during the Late Glacial. *Philosophical Transactions of the Royal Society A*, *381*(2261), 20220206. https://doi.org/10.1098/rsta.2022.0206

Brehm, N., Bayliss, A., Christl, M., Synal, H., Adolphi, F., Beer, J., et al. (2021). Eleven-year solar cycles over the last millennium revealed by radiocarbon in tree rings. *Nature Geoscience*, *14*(1), 10–15. https://doi.org/10.1038/s41561-020-00674-0

Büntgen, U., Wacker, L., Galvan, J., Arnold, S., Arseneault, D., Baillie, M., et al. (2018). Tree rings reveal globally coherent signature of cosmogenic radiocarbon events in 774 and 993 CE. *Nature Communications*, *9*(1), 3605. https://doi.org/10.1038/s41467-018-06036-0

Calisto, M., Usoskin, I., & Rozanov, E. (2013). Influence of a Carrington-like event on the atmospheric chemistry, temperature and dynamics: Revised. *Environmental Research Letters*, *8*(4), 045010. https://doi.org/10.1088/1748-9326/8/4/045010

Cliver, E. W., Schrijver, C. J., Shibata, K., & Usoskin, I. G. (2022). Extreme solar events. *Living Reviews in Solar Physics*, *19*(1), 2. https://doi.org/10.1007/s41116-022-00033-8

Desai, M., & Giacalone, J. (2016). Large gradual solar energetic particle events. *Living Reviews in Solar Physics*, *13*(1), 3. https://doi.org/10.1007/s41116-016-0002-5

Golubenko, K., Rozanov, E., Mironova, I., Karagodin, A., & Usoskin, I. (2020). Natural sources of ionization and their impact on atmospheric electricity. *Geophysical Research Letters*, *47*(12), e88619. https://doi.org/10.1029/2020GL088619

Golubenko, K., Usoskin, I., Bard, E., Koldobskiy, S., & Rozanov, E. (2026). Full dynamical model (SOCOL:14C-Ex) of ^{14}C atmospheric production and transport in application to Miyake events. *Radiocarbon*, 1–22. https://doi.org/10.1017/RDC.2026.10236

Golubenko, K., Usoskin, I., Rozanov, E., & Bard, E. (2025). New SOCOL:14C-Ex model reveals that the Late-Glacial radiocarbon spike in 12350 BC was caused by the record-strong extreme solar storm. *Earth and Planetary Science Letters*, *661*, 119383. https://doi.org/10.1016/j.epsl.2025.119383

Hathaway, D. H. (2015). The solar cycle. *Living Reviews in Solar Physics*, *12*(1), 4. https://doi.org/10.1007/lrsp-2015-4

Heaton, T., Bard, E., Bayliss, A., Blaauw, M., Bronk Ramsey, C., Reimer, P., et al. (2024). Extreme solar storms and the quest for exact dating with radiocarbon. *Nature*, *633*(8029), 306–317. https://doi.org/10.1038/s41586-024-07679-4

Hessl, A. E., Richardson, A. D., Filwett, R., Andreu-Hayles, L., Walker, M., Oelkers, R., et al. (2026). Carbon uptake, storage, and allocation patterns contribute to blurring of annual ^{14}C signals in tree rings. *New Phytologist*, *250*(6), 3584–3600. https://doi.org/10.1111/nph.70868

Koldobskiy, S. A., Raukunen, O., Vainio, R., Kovaltsov, G., & Usoskin, I. (2021). New reconstruction of event-integrated spectra (spectral fluences) for major solar energetic particle events. *Astronomy and Astrophysics*, *647*, A132. https://doi.org/10.1051/0004-6361/202040058

Kovaltsov, G., Mishev, A., & Usoskin, I. (2012). A new model of cosmogenic production of radiocarbon ^{14}C in the atmosphere. *Earth and Planetary Science Letters*, *337*, 114–120. https://doi.org/10.1016/j.epsl.2012.05.036

Mekhaldi, F., Adolphi, F., Herbst, K., & Muscheler, R. (2021). The signal of solar storms embedded in cosmogenic radionuclides: Detectability and uncertainties. *Journal of Geophysical Research: Space Physics*, *126*(8), e2021JA029351. https://doi.org/10.1029/2021JA029351

Mekhaldi, F., Muscheler, R., Adolphi, F., Aldahan, A., Beer, J., McConnell, J., et al. (2015). Multiradionuclide evidence for the solar origin of the cosmic-ray events of AD 774/5 and 993/4. *Nature Communications*, *6*(1), 8611. https://doi.org/10.1038/ncomms9611

Miyahara, H., Tokanai, F., Moriya, T., Takeyama, M., Sakurai, H., Ohyama, M., et al. (2022). Recurrent large-scale solar proton events before the onset of the wolf grand solar minimum. *Geophysical Research Letters*, *49*(5), e2021GL097201. https://doi.org/10.1029/2021gl097201

Miyake, F., Jull, A., Kimura, K., Molnar, M., Moriya, T., Myglan, V., et al. (2026). Reassessment of a cosmic ray increase event in 1279/1280 CE using carbon-14 records of tree rings. *Philosophical Transactions of the Royal Society A*. https://doi.org/10.1098/rsta.2025.0264

Miyake, F., Nagaya, K., Masuda, K., & Nakamura, T. (2012). A signature of cosmic-ray increase in ad 774-775 from tree rings in Japan. *Nature*, *486*(7402), 240–242. https://doi.org/10.1038/nature11123

F. Miyake, I. Usoskin, & S. Poluianov (2020). *Extreme solar particle storms: The hostile sun*. IOP Publishing. https://doi.org/10.1088/2514-3433/ab404a

Paleari, C., Mekhaldi, F., Adolphi, F., Christl, M., Vockenhuber, C., Gautschi, P., et al. (2022). Cosmogenic radionuclides reveal an extreme solar particle storm near a solar minimum 9125 years bp. *Nature Communications*, *13*(1), 214. https://doi.org/10.1038/s41467-021-27891-4

Panovska, S., Poluianov, S., Gao, J., Korte, M., Mishev, A., Shprits, Y. Y., & Usoskin, I. (2023). Effects of global geomagnetic field variations over the past 100,000 years on cosmogenic radionuclide production rates in the Earth's atmosphere. *Journal of Geophysical Research: Space Physics*, *128*(8), e2022JA031158. https://doi.org/10.1029/2022JA031158

Panyushkina, I. P., Jull, A., Molnár, M., Varga, T., Kontul', I., Hantemirov, R., et al. (2024). The timing of the ca-660 BCE Miyake solar-proton event constrained to between 664 and 663 BCE. Commun. *Earth and Environment*, *5*(1), 454. https://doi.org/10.1038/s43247-024-01618-x

Pavón-Carrasco, F. J., Osete, M. L., Torta, J. M., & De Santis, A. (2014). A geomagnetic field model for the Holocene based on archaeomagnetic and lava flow data. *Earth and Planetary Science Letters*, *388*, 98–109. https://doi.org/10.1016/j.epsl.2013.11.046

Poluianov, S., Kovaltsov, G. A., Mishev, A. L., & Usoskin, I. G. (2016). Production of cosmogenic isotopes ^{7}Be, ^{10}Be, ^{14}C, ^{22}Na, and ^{36}Cl in the atmosphere: Altitudinal profiles of yield functions. *Journal of Geophysical Research: Atmospheres*, *121*(13), 8125–8136. https://doi.org/10.1002/2016JD025034

Reimer, P., Austin, W., Bard, E., Bayliss, A., Blackwell, P., Ramsey, C., et al. (2020). The INTCAL20 Northern Hemisphere radiocarbon age calibration curve (0-55 CAL KBP). *Radiocarbon*, *62*(4), 725–757. https://doi.org/10.1017/RDC.2020.41

Roth, R., & Joos, F. (2013). A reconstruction of radiocarbon production and total solar irradiance from the Holocene ^{14}C and CO_2 records: Implications of data and model uncertainties. *Climate of the Past*, *9*(4), 1879–1909. https://doi.org/10.5194/cp-9-1879-2013

Sukhodolov, T., Usoskin, I., Rozanov, E., Asvestari, E., Ball, W., Curran, M., et al. (2017). Atmospheric impacts of the strongest known solar particle storm of 775 AD. *Scientific Reports*, *7*(1), 45257. https://doi.org/10.1038/srep45257

Usoskin, I. G. (2023). A history of solar activity over Millennia. *Living Reviews in Solar Physics*, *20*(1), 2. https://doi.org/10.1007/s41116-023-00036-z

Usoskin, I. G., Alanko-Huotari, K., Kovaltsov, G. A., & Mursula, K. (2005). Heliospheric modulation of cosmic rays: Monthly reconstruction for 1951–2004. *Journal of Geophysical Research*, *110*(A12), A12108. https://doi.org/10.1029/2005JA011250

Usoskin, I. G., Gallet, Y., Lopes, F., Kovaltsov, G. A., & Hulot, G. (2016). Solar activity during the Holocene: The Hallstatt cycle and its consequence for grand minima and maxim. *Astronomy and Astrophysics*, *587*, A150. https://doi.org/10.1051/0004-6361/201527295

Usoskin, I. G., Gil, A., Kovaltsov, G. A., Mishev, A. L., & Mikhailov, V. V. (2017). Heliospheric modulation of cosmic rays during the neutron monitor era: Calibration using PAMELA data for 2006-2010. *Journal of Geophysical Research: Space Physics*, *122*(4), 3875–3887. https://doi.org/10.1002/2016JA023819

Usoskin, I. G., Koldobskiy, S. A., Kovaltsov, G. A., Rozanov, E. V., Sukhodolov, T. V., Mishev, A. L., & Mironova, I. A. (2020). Revisited reference solar proton event of 23 February 1956: Assessment of the cosmogenic-isotope method sensitivity to extreme solar events. *Journal of Geophysical Research: Space Physics*, *125*(6), e27921. https://doi.org/10.1029/2020JA027921

Usoskin, I. G., & Kovaltsov, G. (2021). Mind the gap: New precise ^{14}C data indicate the Nature of extreme solar particle events. *Geophysical Research Letters*, *48*(17), e94848. https://doi.org/10.1029/2021GL094848

Usoskin, I. G., Kromer, B., Ludlow, F., Beer, J., Friedrich, M., Kovaltsov, G. A., et al. (2013). The AD775 cosmic event revisited: The Sun is to blame. *Astronomy and Astrophysics*, *552*, L3. https://doi.org/10.1051/0004-6361/201321080

Usoskin, I. G., Miyake, F., Baroni, M., Brehm, N., Dalla, S., Hayakawa, H., et al. (2023). Extreme solar events: Setting up a paradigm. *Space Science Reviews*, *219*(8), 73. https://doi.org/10.1007/s11214-023-01018-1

Usoskin, I. G., Solanki, S. K., & Kovaltsov, G. A. (2007). Grand minima and maxima of solar activity: New observational constraints. *Astronomy and Astrophysics*, *471*(1), 301–309. https://doi.org/10.1051/0004-6361:20077704

Usoskin, I. G., Solanki, S. K., Krivova, N., Hofer, B., Kovaltsov, G. A., Wacker, L., et al. (2021). Solar cyclic activity over the last millennium reconstructed from annual ^{14}C data. *Astronomy and Astrophysics*, *649*, A141. https://doi.org/10.1051/0004-6361/202140711

Uusitalo, J. (2026). Tree physiology is essential for interpreting Miyake events. *New Phytologist*, *250*(6), 3513–3515. (in press). https://doi.org/10.1111/nph.71002

Wu, C. J., Usoskin, I. G., Krivova, N., Kovaltsov, G. A., Baroni, M., Bard, E., & Solanki, S. K. (2018). Solar activity over nine millennia: A consistent multi-proxy reconstruction. *Astronomy and Astrophysics*, *615*, A93. https://doi.org/10.1051/0004-6361/201731892